ChemComm

FEATURE ARTICLE

View Article Online
View Journal

Cite this: DOI: 10.1039/d6cc00206d

BASHY dyes as modular chromophores for multifaceted biorelevant applications: from imaging to photodynamic therapy

Fábio M. F. Santos,*[a] Francisco G. Blandón-Cumbreras,[b] Uwe Pischel*[b] and Pedro M. P. Gois*[a]

The multifactorial nature of biological systems and the ongoing effort to elucidate their underlying mechanisms have driven the demand for advanced fluorescent probes with high sensitivity and functional adaptability. To meet these challenges, multicomponent reactions (MCRs) offer a powerful synthetic strategy for the straightforward design of structurally diverse fluorophores with tunable chemical and photophysical properties. In this context, the boronic-acid derived salicylidenehydrazone (BASHY) platform has emerged as a versatile class of dyes featuring π-conjugated ligands coordinated to an sp^3-hybridized boron centre. This molecular design yields fluorophores with polarity-sensitive emission and significant photostability. The modular scaffold allows the systematic tuning of photophysical properties, while preserving fluorescence efficiency upon derivatization. BASHY dyes display exceptional performance in bioimaging, enabling the labeling of lipid droplets (LDs), astrocytes, apoptotic cells, and myelin debris in *in vivo* demyelination models. The BASHY framework also supports energy-transfer cassettes (ETCs) with nearly quantitative energy transfer efficiencies and offers compatibility with fluorescence lifetime imaging microscopy (FLIM). Beyond imaging, BASHY dyes act as highly efficient singlet-oxygen photosensitizers (PSs) with potential applications in photodynamic therapy (PDT). Furthermore, specifically designed conjugates integrate both imaging and therapeutic functions, displaying potent cytotoxicity. In this review, we discuss the evolution of the BASHY platform and its applications that position these dyes as promising candidates for next-generation imaging and theranostic agents.

Received 11th January 2026,
Accepted 27th April 2026

DOI: 10.1039/d6cc00206d

rsc.li/chemcomm

[a] *Research Institute for Medicines (iMed.ULisboa), Faculty of Pharmacy, Universidade de Lisboa, Lisbon 1649-003, Portugal*
[b] *CIQSO – Centre for Research in Sustainable Chemistry and Department of Chemistry, University of Huelva, Campus de El Carmen, E-21071 Huelva, Spain. E-mail: uwe.pischel@diq.uhu.es*

Fábio M. F. Santos

Fábio M. F. Santos is currently a junior researcher in the Chemical Biology group at iMed.Ulisboa in the Faculty of Pharmacy of the University of Lisbon (FFUL). He obtained his BSc in Biochemistry from NOVA School of Science and Technology in 2009 and his MSc in Pharmaceutical and Medicinal Chemistry from FFUL in 2012. He then completed his PhD in Pharmacy at FFUL in 2008 under the supervision of Prof. Pedro Gois, followed by a two-year postdoctoral position at iMed.Ulisboa. His current research focuses on the design of modular, tunable, and responsive platforms for advanced bioimaging and therapeutic applications.

Francisco G. Blandón-Cumbreras

Francisco G. Blandón-Cumbreras (1999, Spain) received his Bachelor's and Master's degrees in Chemistry from the University of Huelva (Spain) in 2021 and 2022, respectively. He is currently pursuing a PhD at the Center for Research in Sustainable Chemistry, University of Huelva, under the guidance of Prof. Uwe Pischel, working on the synthesis and photochemistry of molecular switches and novel fluorophore architectures.

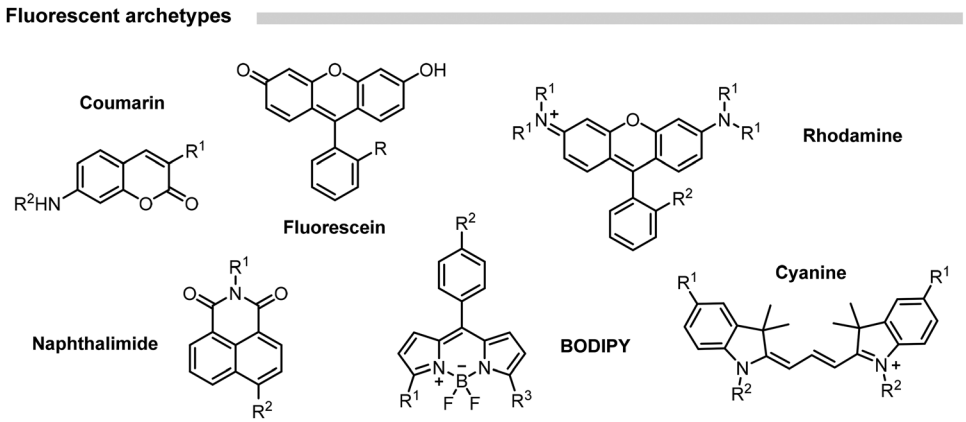

Fig. 1 Representative fluorescent frameworks employed in bioimaging.

Introduction

Fluorescent dyes are an invaluable class of functional molecules, widely used to study the intricacies of biological processes. In recent years, considerable efforts have been made to expand the chemical space of these compounds by designing chromophores with structural and photophysical properties that are tailored for bioimaging.[1–18]

Several classes of small organic frameworks, such as coumarins, naphthalimides, fluoresceins, rhodamines, BODIPYs or cyanines (Fig. 1), have gained prominence in this field, mainly due to their suitable biocompatibility and exceptional photophysical/photochemical properties, including high photostability, brightness, and quantum yields. Owing to these properties, these dyes have been widely used to enhance our ability to visualize and follow complex biological processes with high sensitivity and specificity.[19,20]

However, the use of these dyes in specific applications often requires the adaptation of the chromophore architecture to meet concrete biological requirements. This task is particularly challenging, because molecular diversification can affect the electronic structure and consequently the photophysical properties of the chromophore. Therefore, the development of synthetic methods to create easily tuneable dyes with predictable fluorescence properties is critical to advancing the imaging of complex biological processes.

The high structural diversity offered by multicomponent reactions (MCRs) can be a particularly useful strategy, either for the diversification of functional fluorescent molecules (scaffold approach) or for the discovery of novel π-conjugated frameworks (chromogenic approach). Müller and co-workers have comprehensively reviewed this subject, showcasing various examples of valuable MCRs, including Ugi, Biginelli, Debus–Radziszewski, and Groebke–Blackburn–Bienaymé (GBB), among others (Fig. 2A).[21,22] One noteworthy example of a powerful application of MCRs in chromophore synthesis is the development of PyrAtes by Maulide and co-workers in 2024. This novel fluorophore class features an imidazo[1,2-*a*]pyridinium core,

Uwe Pischel

Uwe Pischel (1973, Germany) has been a Full Professor of Organic Chemistry at the University of Huelva (Spain) since 2019. He studied Chemistry at the Technical University Dresden and the Humboldt-University Berlin and obtained his PhD in Photochemistry from the University of Basel under the guidance of Prof. Werner M. Nau in 2001. His research interests include molecular switches, supramolecular (photo) chemistry, and the development of new fluorophores. Among other honors, he is the recipient of the Grammaticakis-Neumann Prize (2013) of the Swiss Chemical Society and the Ignacio-Ribas Medal of the Organic Chemistry Division of the Spanish Royal Society of Chemistry (2022).

Pedro M. P. Gois

Gois studied chemistry at the New University of Lisbon, where he obtained his PhD in Organic Chemistry in 2005 under the supervision of Carlos Afonso. After postdoctoral research at the University of Sussex (Geoffrey N. Cloke), University College London (Stephen Caddick), and Instituto Superior Técnico (Carlos Afonso), he joined the Faculty of Pharmacy of the University of Lisbon in 2008. He is currently an Associate Professor with Habilitation at FFUL and Coordinator of iMed.ULisboa, where he leads the Chemical Biology Laboratory. His distinctions include recognition as an Emerging and Pioneering Investigator by Chemical Communications and the Vicente Seabra Medal – SPQ.

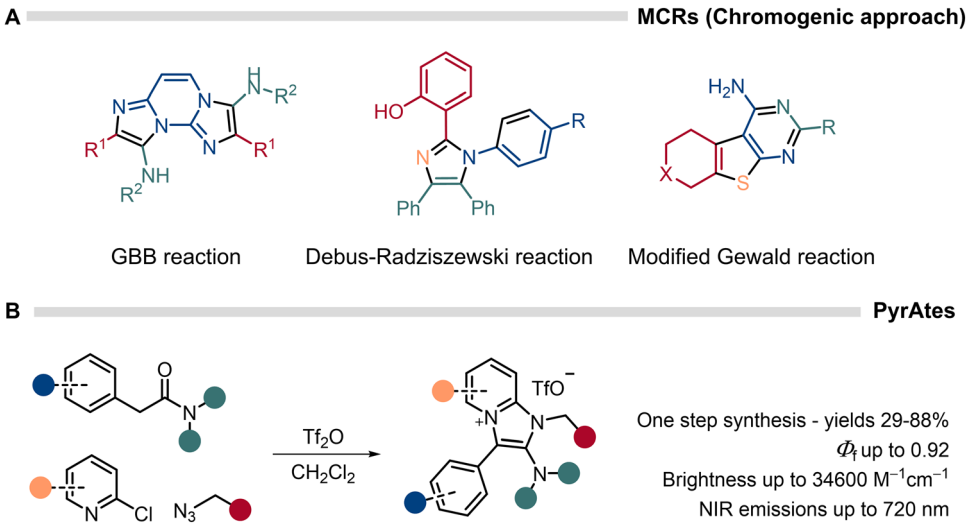

Fig. 2 (A) Selected examples of MCRs applied in the discovery of novel π-conjugated systems; (B) multicomponent synthesis of PyrAtes and some of their photophysical properties.

exhibiting remarkable photophysical properties and potential for live-cell imaging applications (Fig. 2B).[23] Despite some scattered successful examples, the current use of MCRs predominantly focuses on the structural diversification of existing chromophores. Only a limited number of MCRs have been reported to directly generate fluorescent cores with photophysical properties suitable for bioimaging applications.[22]

Boron is a prevalent element in the structure of many chromophores and the success of the BODIPY dyes[24] led to the discovery of numerous fluorescent architectures with bidentate ligands tethered by a central boron atom that is coordinated to fluoride or aromatic moieties. In many of these chromophores, the boron atom plays a crucial role in improving ligand stability, dye planarity, conjugation, and charge transfer throughout the π system.[25] However, boronic acids (BAs), one of the most versatile reagents in modern synthesis, have generally been overlooked as tethers for the construction of fluorescent dyes. This restricted applicability can be rationalized by the following factors: (I) sp^2-hybridized boron complexes are highly reversible under aqueous conditions,[26] which may limit their suitability for advanced bioimaging applications; (II) sp^3-hybridized boron complexes are known to be more stable;[27] however, their tetrahedral geometry forces substituents out of the plane of conjugation, potentially compromising the chromophores' photophysical characteristics (Fig. 3A).[28,29]

BAs exhibit rich coordination chemistry,[30] are responsive to different physiological stimuli, and are readily available in a huge structural diversity, which has allowed the preparation of a plethora of materials for applications as diverse as sensing of carbohydrate[31–33] and anions,[31,33,34] non-linear optics,[28,35–38] drug delivery[39] or the construction of biomaterials.[40,41] Encouraged by this functional and structural diversity, in 2016 we initiated a program to explore BAs as building blocks in MCRs for the construction of chromophores.[42] The motivation for this work was not only to gain access to the chemical space of dyes for bioimaging, but also, equally importantly, to design modular and responsive chromophores that can elucidate the intricacies of biological processes, critical to disease detection and monitoring.[43,44]

Unveiling and structural diversification of the BASHY platform

The discovery of BASHY dyes

Our aim was to design multicomponent chromophores using BAs as a component and conformational lock. Therefore, we established a design principle: the use of ligands with donor and acceptor groups to generate a π-conjugated system capable of coordinating the BA. To this end, we investigated the coordination of Schiff-base ligands with BAs (Fig. 3B). Unfortunately, the prepared boronates exhibited very poor photophysical properties, which was in accordance with earlier observations of Waksman and co-workers.[29] However, when phenylglyoxylic acid was selected as the acceptor group and bridged to the donor group *via* a hydrazone functionality, a fluorescent BASHY was obtained in nearly quantitative yield (Fig. 3C).[42]

It is noteworthy that since the discovery of BASHY dyes, several multicomponent and fluorescent BA-based frameworks (Fig. 4) have been developed, featuring red/near-infrared absorption,[45,46] solid-state fluorescence,[45–51] stimuli-responsive fluorescence,[47–49,52–56] and aggregation-induced emission.[50,54,57–59] These chromophores have also shown promising potential for cell bioimaging,[53] including the staining of lipid droplets (LDs),[51,58] lysosomes,[50] mitochondria,[45,46,50] and the endoplasmic reticulum.[49]

The photophysical evaluation of the first generation of BASHY dyes revealed a pronounced intramolecular charge-transfer (ICT) character with a polarity-sensitive green-to-yellow emission, high emission quantum yields (up to 0.6) in nonpolar environments, high brightness (up to 54 000 M^{-1} cm^{-1}), large Stokes shifts (up to 100 nm), and high photostability. In addition to these photophysical properties, the BASHY modular architecture offers various positions

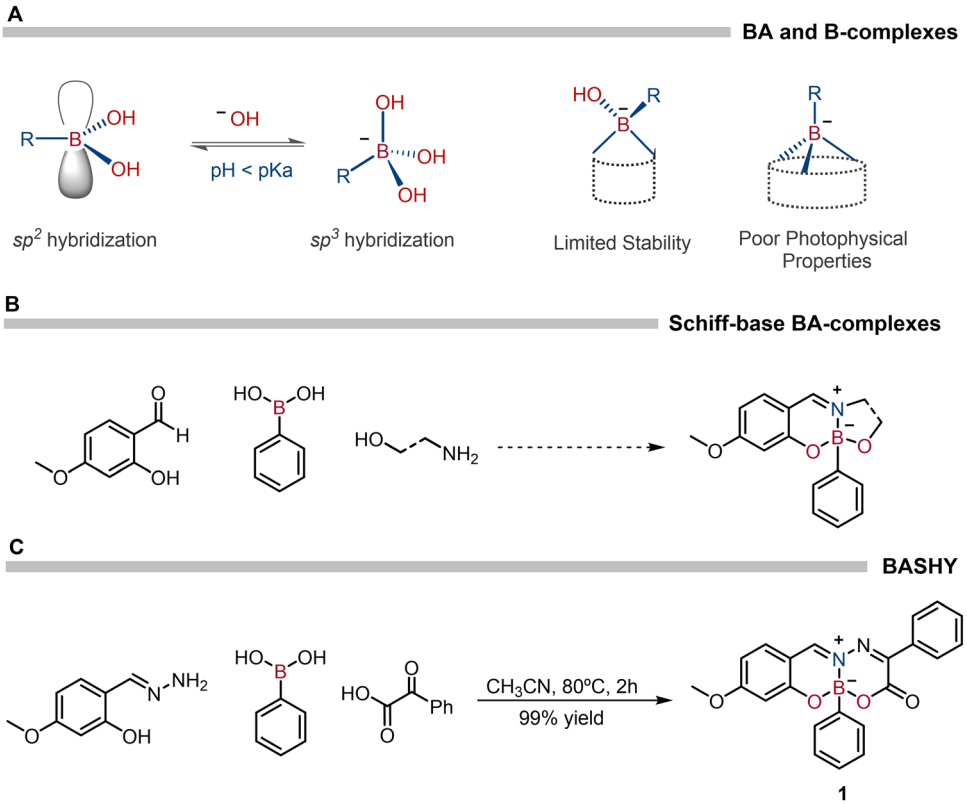

Fig. 3 (A) BA hybridization states and chelation with bi- and tri-dentate ligands; (B) Schiff-base tetrahedral BA-complexes; and (C) modular synthesis of BASHY dye **1**.

for structural diversification and optimization of the photophysical properties (Fig. 4; moieties **A–D**). These will be briefly illustrated in the following sections.

Donor component (moiety A)

Investigating the influence of the substitution at the **A** position (Fig. 4), we observed that dyes with a stronger electron-donating *N*,*N*-diethylamino group exhibited a further red-shift in absorption and emission when compared to methoxy-substituted dyes (Fig. 5).[42] For this reason, the *N*,*N*-diethylamino group has become our prime choice for the electron-donor substituent in the structural diversification of subsequent generations of BASHY dyes.

Acceptor component (moiety B)

The **B** moiety (Fig. 4), located on the opposite end of the salicylidenehydrazone backbone, was used to fine-tune the

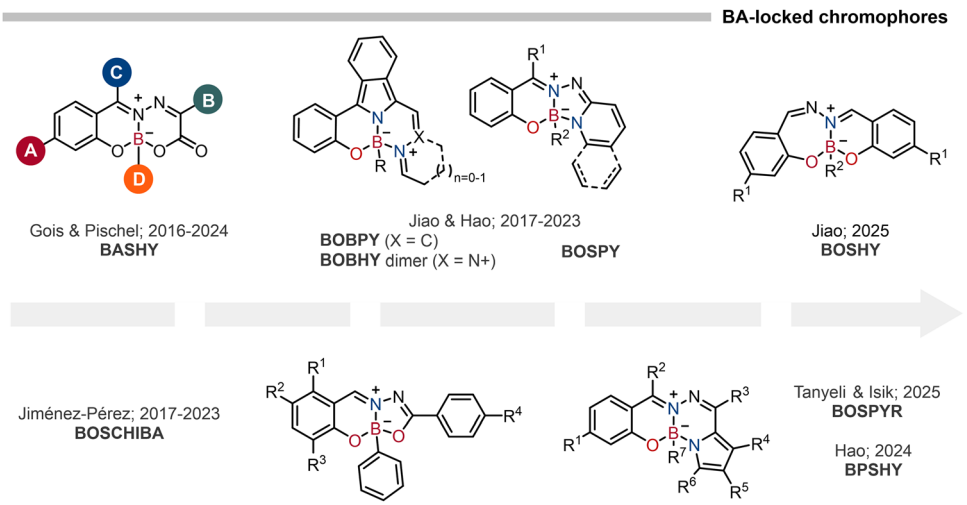

Fig. 4 Selected examples of fluorescent BA-locked frameworks.

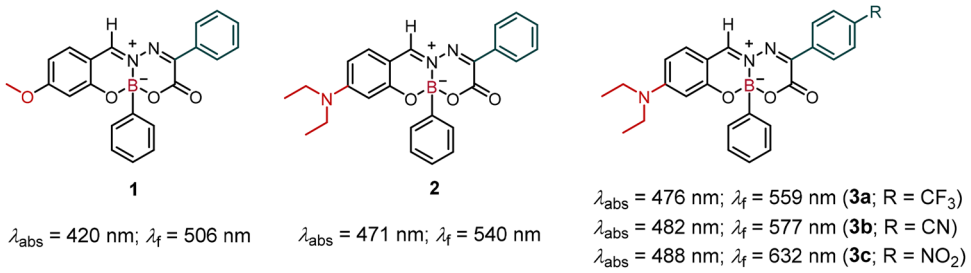

Fig. 5 Structural variation of the donor and acceptor moieties in the BASHY platform. The maxima of the UV/vis absorption and emission spectra are provided.

Table 1 Photophysical properties of **2** and **3a–c** in aerated organic solvents

	2	3a	3b	3c
Toluene (P = 2.4)				
$\lambda_{abs,max}$ (nm)	471	478	484	489
$\lambda_{f,max}$ (nm)	508	516	525	535
Φ_f	0.60	0.65	0.57	0.55
THF (P = 4.0)				
$\lambda_{abs,max}$ (nm)		478	483	489
$\lambda_{f,max}$ (nm)		537	549	579
Φ_f		0.30	0.28	0.23
CH_3CN (P = 5.8)				
$\lambda_{abs,max}$ (nm)	471	476	482	488
$\lambda_{f,max}$ (nm)	540	559	577	632
Φ_f	0.08	0.05	0.05	<0.01

push–pull (ICT) character of BASHY dyes *via* the introduction of electron-acceptor groups. Thus, the increase of the electron-withdrawing properties of the phenyl *para*-substituent [Hammett constant (σ_p) = 0 (H; **2**), 0.54 (CF_3; **3a**), 0.66 (CN; **3b**), and 0.78 (NO_2; **3c**)][60] led to a pronounced red-shift of the emission maximum of the BASHY platform (see Fig. 5). Additionally, these fluorophores exhibit solvatofluorochromic character, with pronounced bathochromic shifts of the emission spectrum in solvents of increased polarity (Table 1).[61] However, this comes at the cost of reduced fluorescence quantum yields. This may be explained by the energy-gap law, predicting more dominant nonradiative deactivation of energetically lower lying excited singlet states. The overall solvatofluorochromic behavior corroborates the involvement of ICT in the excited singlet state of these BASHY dyes.

Initial theoretical studies of the BASHY platform using the density-functional-theory (DFT) methodology pointed to the involvement of a pronounced ICT character of the excited state, in agreement with the observed solvatofluorochromism.[42] In a detailed follow-up theoretical study, Jacquemin and co-workers confirmed the charge-transfer characteristics, but pointed out an interesting mixing with cyanine-like properties.[62] This observation prompted us to further exacerbate the cyanine-like character with the conjugative π-extension of the acceptor component (**4a–c**, Fig. 6) and thereby to explore this photomechanistic continuum for the BASHY dye family.

In comparison to **4a**, dyes **4b** and **4c** (Fig. 6) feature a polymethine backbone (Cy-BASHY). These BASHY dyes display red-shifted UV/vis absorption [λ_{abs} (DMSO): **4a** – 480 nm; **4b** – 507 nm and **4c** – 525 nm] and fluorescence emission [λ_f (DMSO): **4a** – 567 nm; **4b** – 589 nm and **4c** – 599 nm], high brightness (up to 16 000 M^{-1} cm^{-1}), significant Stokes shifts (about 80 nm), and reasonable quantum yields in highly polar solvents [Φ_f (DMSO): **4a** – 0.13; **4b** – 0.19 and **4c** – 0.24].[63] The observed dependence of the absorption and emission maxima on the π-conjugation length is in clear accordance with the theoretically expected cyanine-like character of these dyes; *cf.* König's rule.

The mapping of the increased π-extension of the salicylidene-hydrazone backbone into a more significant cyanine-like character was further confirmed in DFT studies of the BASHY dyes **4a–c**.[64] The calculation of the D index, which is the distance between the hole and electron barycenters, showed significant ICT character for **4a** (D = 3.176 Å). However, this parameter decreased gradually for **4b** (D = 1.639 Å) and indicated full cyanine-like behavior for **4c** (D = 0.639 Å).

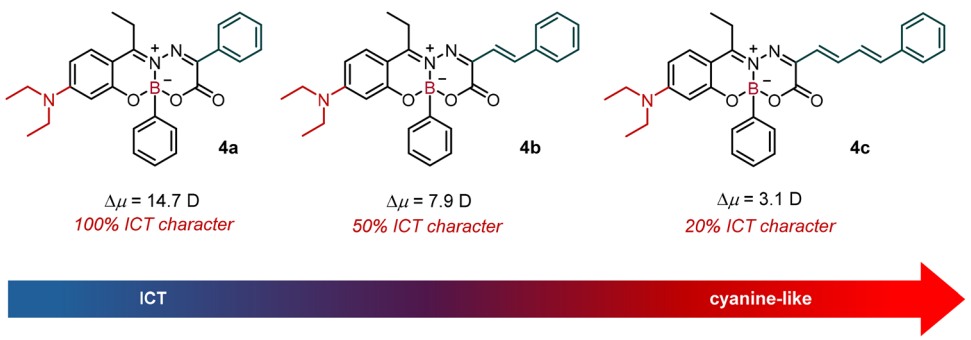

Fig. 6 Dipole moment and ICT character of BASHY dyes upon π-extension of the salicylidenehydrazone ligand backbone.

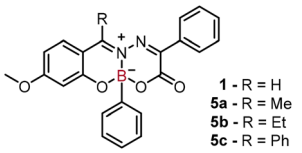

Fig. 7 BASHY dyes with structural variation at the iminium carbon substituent.

Iminium carbon substituent (moiety C)

This substituent (moiety **C**; Fig. 4) of the salicylidenehydrazone ligand plays a very important role in the BASHY architecture. Generally, bulkier groups at the iminium carbon confer higher hydrolytic stability to the complexes [$t_{1/2}$ in 10 mM ammonium acetate solution (pH 7): **1** – 2 min; **5a** – 18 min; **5b** – 40 min and **5c** – 185 min] (Fig. 7).[63]

In addition to the stabilization of the iminium electrophilic centre, substitution at this position with a *p*-*N*,*N*-diethylaminophenyl group (**6a–c**; Fig. 8) can also induce fluorescence quenching by photoinduced electron transfer (PeT), which can be reverted by the addition of an acid in an organic solvent (OFF–ON fluorescence switching; Fig. 8). The resulting emission is observed in the green-to-orange spectral region (maxima at 520–590 nm in CH_3CN). In contrast, under physiological pH conditions (phosphate-buffered saline – PBS; pH 7), the PeT process is inherently deactivated, thereby enabling the observation of fluorescence in the red-to-NIR region (maxima at 650–680 nm).[65]

BA component (moiety D)

The BA moiety (**D** in Fig. 4) plays a pivotal role in the BASHY architecture as the salicylidenehydrazone ligand itself is essentially non-fluorescent and it is only upon condensation with BA that the typical fluorescence of BASHY is observed. Despite this important role of the BA component as a conformational lock, the emission properties of the BASHY dyes are widely invariant with the substitution pattern of the BA aryl moiety. This appears to be a direct consequence of the out-of-plane, non-conjugative orientation of the BA aryl residue, in accordance with the sp^3 character of the boron centre. This situation allows the modification of the dyes in an electronically innocent way (Fig. 9). The preparation of dimers (such as dye 7), in which both halves do not communicate electronically, is one example. Thus, dye 7 retains the fluorescence properties of **2** (Fig. 5), but the molar absorption coefficient is almost doubled [CH_3CN: 103 900 M^{-1} cm^{-1} (7) *versus* 60 000 M^{-1} cm^{-1} (**2**)].[42] This was confirmed by DFT calculations, which clearly confirmed that both chromophoric units feature independent transitions, involving degenerate frontier molecular orbitals.[42] Similar conclusions were drawn from DFT calculations of a heterobichromophoric dyad featuring BASHY and BODIPY moieties (see below).[66]

Other examples are the preparation of BASHY dyes **8–10** (Fig. 9), which were used, respectively, as a clickable fluorescent tag for annexin V, as a stain for astrocytes, and as a photosensitizer (PS) for photodynamic therapy (PDT); see below.[61,63,67]

As mentioned above, the substituent at the iminium carbon confers steric and electronic protection to this electrophilic centre, which affects the hydrolytic stability of these complexes positively. However, in order to evaluate the hydrolytic stability of BASHY dyes in a holistic manner, including synergistic effects, we developed a multivariate linear-free energy relationship (mLFER) model.[68] For this, a library of twenty structurally diverse BASHY dyes was employed. This resulted in the prediction of an optimized structure with elevated hydrolytic stability and application potential for prolonged bioimaging experiments (Fig. 10). The identified lead structure, compound **11**, revealed remarkable stability in PBS at pH 7.4 ($t_{1/2}$ = 95 h) and in DMEM cultivation medium ($t_{1/2}$ = 128 h). Additionally, in blood plasma, no measurable degradation was observed over 70 h. Interestingly, the *o*-phenyl substituent of the BA moiety was found to play a crucial role in the hydrolytic stability of this structure. DFT calculations performed on dye **11** corroborated that a steric clash between the i-Bu substituent at the iminium carbon and the *o*-CN phenylboronic acid component limits the nucleophilic attack of water.[68]

Additional insights into the photophysical properties of BASHY dyes

Based on the above outlined factors that impact the photophysical properties and the fine-tuning of the mechanistic

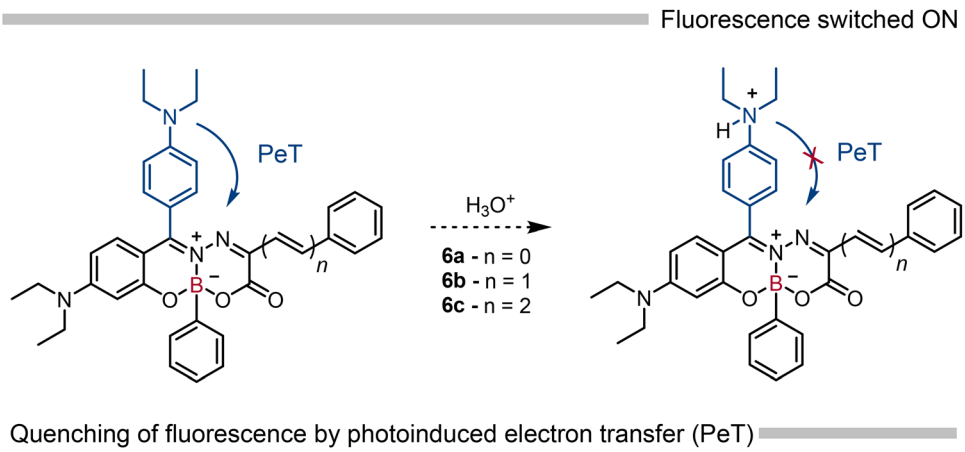

Fig. 8 Fluorescence quenching of BASHY *via* PeT and re-activation under acidic conditions.

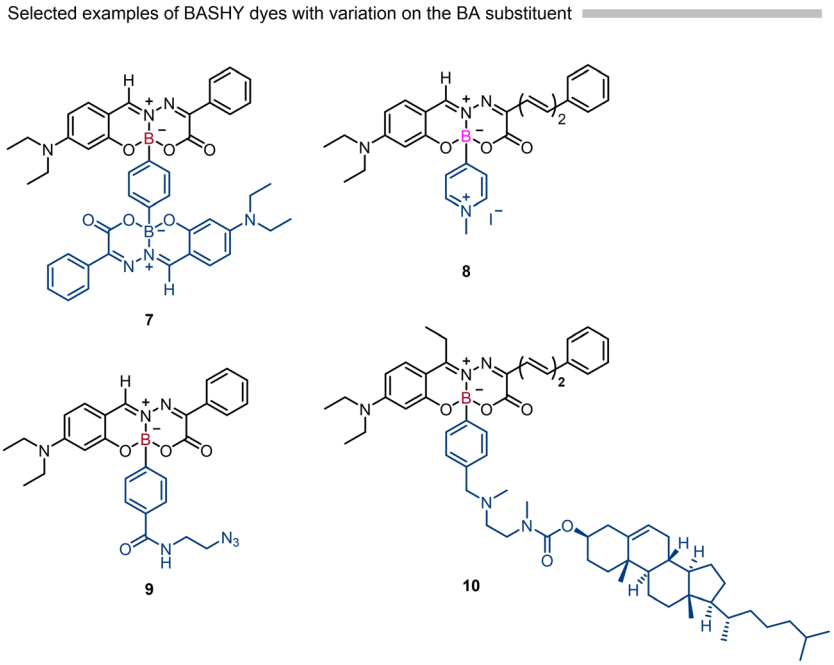

Fig. 9 Examples of the structural diversification of the BA moiety, integrated into the BASHY platform.

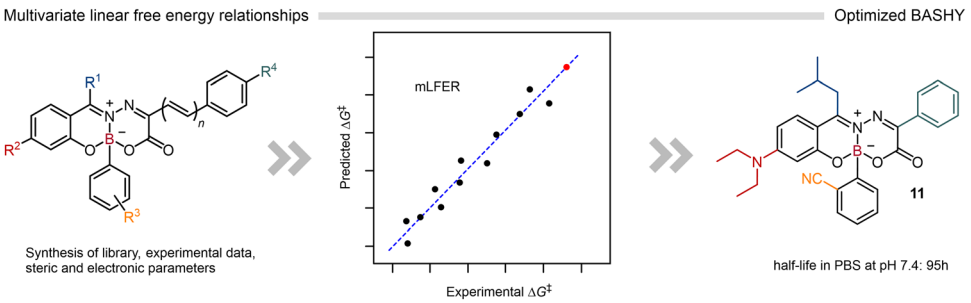

Fig. 10 Workflow for the development of optimized BASHY dyes using mLFER.

A

	λ_f^{2PE} (nm)	σ_2 (GM)
2	508	194 (890 nm), 117 (950 nm)
3a	518	214 (890 nm), 128 (950 nm)
3b	528	176 (890 nm), 164 (970 nm)
3c	537	283 (910 nm), 295 (980 nm)

B

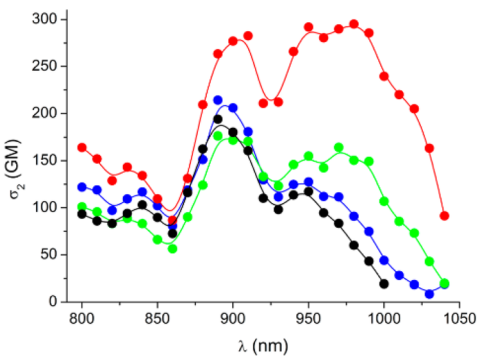

Fig. 11 (A) Photophysical data related to 2PA of dyes **2** and **3a–c** in toluene; (B) 2PA spectra of dyes **2** (black), **3a** (blue), **3b** (green), and **3c** (red) in toluene. Adapted from ref. 61 with permission from American Chemical Society, Copyright 2017.

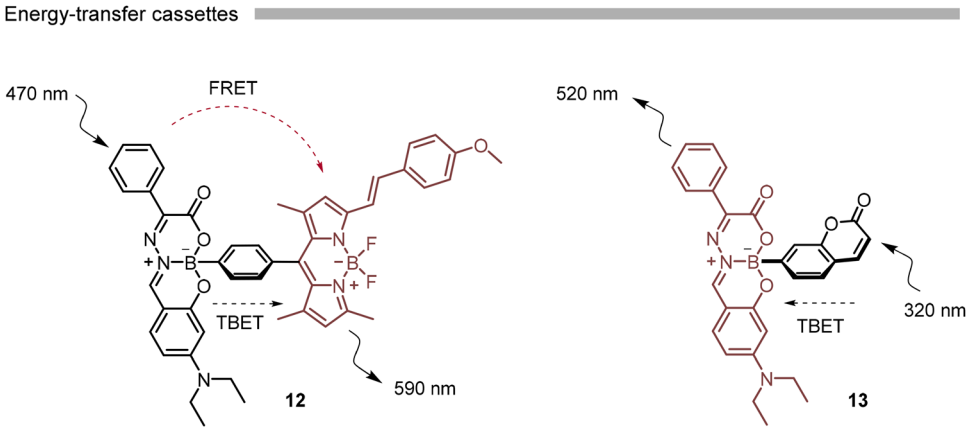

Fig. 12 ETCs **12** and **13** and related mechanisms of energy transfer. Adapted from ref. 66 with permission from John Wiley and Sons, Copyright 2018.

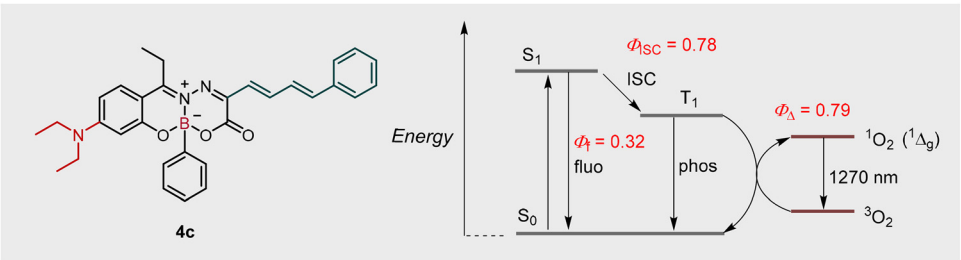

Fig. 13 Proposed excited-state deactivation pathways of BASHY **4c**, including $^1O_2$ generation. Adapted from ref. 64 with permission from American Chemical Society, Copyright 2023.

continuum of BASHY, defined by charge-transfer and cyanine-like character, the dyes were further explored.

Two-photon absorption (2PA) properties

A direct consequence of charge-transfer processes is the possible observation of multi-photon absorption.[69] This was verified for the series of the aforementioned dyes **2** and **3a–c** (Fig. 5). For these dyes, 2PA between *ca.* 900 and 1000 nm was observed with cross sections (σ_2) that reached values of almost 300 GM for dye **3c** and *ca.* 200 GM for the other three dyes (Fig. 11A and B).[61] The two-photon excitation led to the population of the lowest excited singlet state, resulting in the same fluorescence as observed in conventional one-photon spectroscopy.

Circularly polarized luminescence (CPL)

BASHY dyes contain a single stereogenic element, characterized by the asymmetrically substituted boron centre. Hence, the dyes are synthesized as racemic mixtures. While the enantiomers exhibit indistinguishable photophysical properties with respect to their conventional characterization, we anticipated that they could be emitters of CPL. To demonstrate this feature, the racemates of dyes **2** and **3a–c** (Fig. 5) were separated by chiral chromatography and subjected to CPL measurements.[70] The observed luminescence signals coincide with the conventional fluorescence spectra, pointing to the fact that the charge-transfer features are maintained. The observed dissymmetry factors are moderate, *i.e.*, $g_{lum} \approx 3–5 \times 10^{-4}$, albeit in the order of magnitude of related organoboron dyes with similar stereogenic elements.

Energy-transfer cassettes (ETCs)

Building on the notion that BASHY dyes are efficient fluorophores, we further exploited their integration into ETCs. For this purpose, BASHY **2** was linked to a BODIPY dye (dyad **12**) *via* a phenylene spacer or a coumarin (dyad **13**) *via* a single σ-bond (Fig. 12). For ETC **12**, an efficient Förster resonance energy transfer (FRET) process ($\Phi_{FRET} > 0.95$) was observed, with the BASHY dye being the energy donor and the BODIPY dye acting as the acceptor. Indeed, upon selective excitation of the BASHY moiety (between 410 nm and 490 nm), the FRET-sensitization of the characteristic BODIPY emission (at *ca.* 580 nm) was observed. In the case of ETC **13**, it is very reasonable to assume that through-bond energy transfer (TBET) is operative due to the very compact arrangement of both chromophores, this time the BASHY moiety being the energy acceptor. Upon excitation of **13** into the coumarin band (320 nm), BASHY emission (520 nm) was observed, implying a practically quantitative energy-transfer process ($\Phi_{TBET} > 0.95$).[66]

Sensitization of singlet-oxygen ($^1O_2$) formation

For the π-extended dyes **4b** and **4c**, the fluorescence quantum yields in non-polar solvents are substantially lower than for their non-extended counterpart (0.72 for dye **4a** *versus* 0.58 and 0.32 for **4b** and **4c**, respectively, in toluene; Fig. 6). Hence, the

more extended the π-conjugation system, the more competitive non-radiative pathways interfere in the excited singlet-state deactivation. A detailed study revealed that this competition consists mainly of the population of excited triplet states *via* intersystem crossing (ISC). These serve as precursors for the energy-transfer sensitized formation of $^1O_2$. As a result, dye **4c** is especially an excellent $^1O_2$ sensitizer ($\Phi_\Delta \approx 0.8$) in non-polar environments (Fig. 13).[64] This provided the photophysical basis for the use of this dye in advanced PDT applications; see below.

Bioimaging applications of BASHY dyes

BASHY dyes are characterized by their high lipophilicity, a three-dimensional structure imposed by the sp^3-hybridized boron center, and low dark toxicity, as demonstrated in their incubation with healthy cell lines such as dendritic cells (DCs, JAWSII) and human retinal pigment epithelial-1 (RPE-1).[42,64] In our initial evaluation, we clearly observed that the BASHY dyes **2** and **3c** (Fig. 5) rapidly enter the cells, within just 10 minutes of incubation, and tend to accumulate in lipid droplets (LDs),[42] which are spherical cytoplasmic organelles composed of a neutral lipid core that plays a key role in lipid metabolism.[71] This was established by co-localization experiments with the archetypal Nile Red stain. Throughout this study, we never observed the labeling of the cell membrane, which we attributed to the poor ability of this highly three-dimensional structure to intercalate into a more ordered lipidic region.

Myelin debris phagocytosis by microglia during demyelination

The affinity of BASHY dyes for disordered lipid-rich regions was exploited to study microglial activity in multiple sclerosis. This condition is a demyelinating disease of the central nervous system, characterized by the presence of demyelinated regions with accumulated myelin-lipid debris, which are cleared by microglia.[72] We observed that the BASHY dyes **2** and **4a–c** (structures in Fig. 5 and 6) were able to label lipid debris and image the clearance in demyelinated *ex vivo* organotypic cultures and in primary microglial cells.[73] Among the tested BASHY dyes, compound **4a** exhibited superior performance, characterized by strong staining intensity and low background emission. These features enable the clear differentiation between detached myelin debris and intact or early-stage damaged myelin fibres, thereby allowing a more precise visualization of myelin clearance by lesion-associated microglial cells. In addition, BASHY **4a** facilitated the imaging of amoeboid phagocytic microglia (foamy cells) due to its efficacy in labeling myelin debris. Most importantly, BASHY **4a** was also used with an *in vivo* mouse model, where the dye was found in demyelinated areas of the brain of experimental autoimmune encephalomyelitis-induced (EAE) mice (Fig. 14).[73]

Fluorescence lifetime imaging microscopy (FLIM)

Live-cell bioimaging is essential for understanding dynamic cellular processes in real time, providing important insights into the behavior, function, and interactions of cells in their native environment. The use of FLIM[74] is a particularly useful technique in this area, and BASHY **11** (Fig. 10) was recently employed for this purpose in live A549 lung adenocarcinoma cells. The dye exhibits two distinct fluorescence lifetime components (τ_f), namely in vesicles (1.0 ns) and around the perinuclear region (1.9 ns). More importantly, the vesicles associated with the shorter lifetime of **11** are of particular importance in time-lapse imaging, as they have been observed

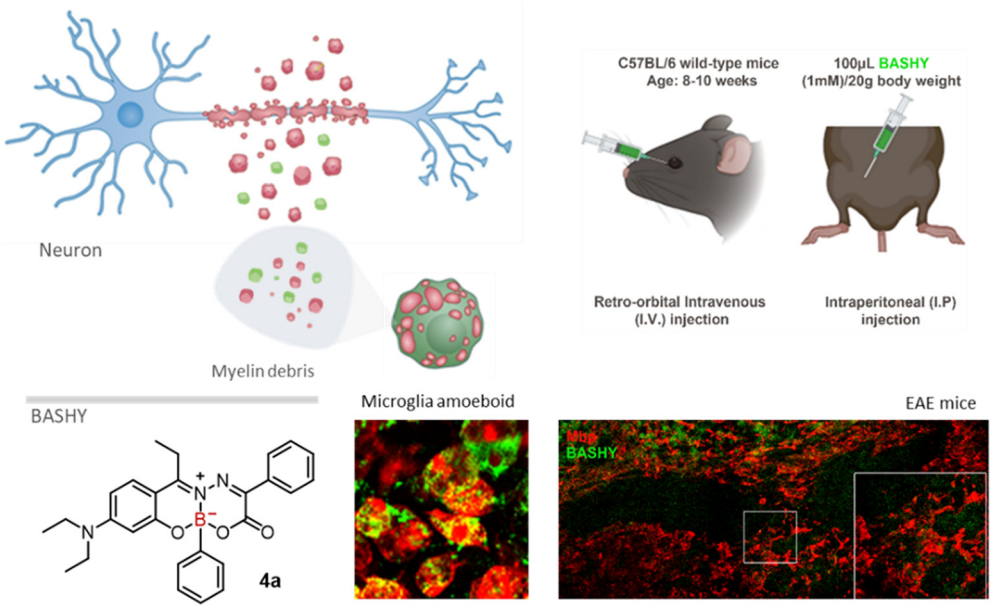

Fig. 14 (A) Demyelination process showing phagocytosis of BASHY-stained myelin debris by amoeboid microglia; (B) *in vivo* evaluation of BASHY administration in experimental autoimmune encephalomyelitis (EAE) mice. Adapted from ref. 73 under the terms and conditions of the Creative Commons Attribution (CC-BY) license, licensee MDPI, 2021.

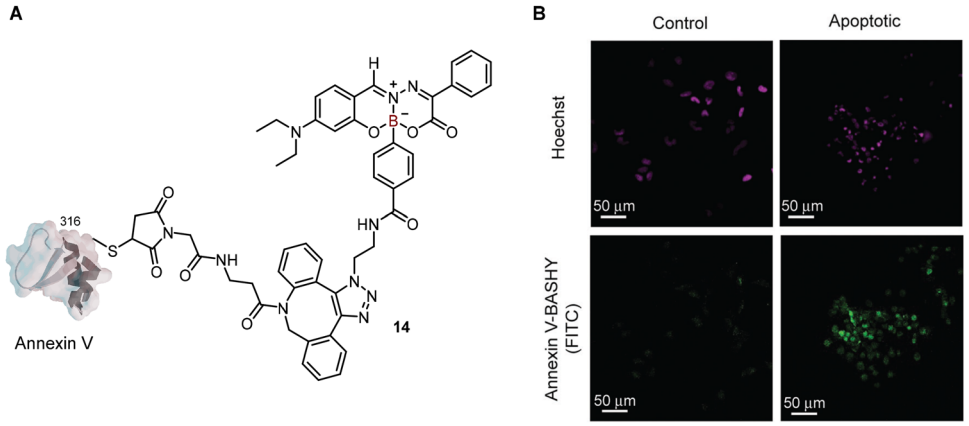

Fig. 15 (A) Structure of annexin V–BASHY conjugate **14**; (B) confocal microscopy images of HeLa cells treated with actinomycin D (apoptotic) or 0.1% DMSO (control), followed by incubation with annexin V–BASHY conjugate **14** (green). Nuclear Hoechst staining (purple). Adapted from ref. 67 with permission from the Royal Society of Chemistry, Copyright 2017.

to be transported within tunneling nanotubes as a means of cell-to-cell communication and content transfer.[68]

An annexin V–BASHY conjugate for the labeling of apoptotic cells

Annexin V has been widely used as a marker of apoptosis due to its ability to bind phosphatidylserine, a phospholipid membrane component, which is translocated from the inner to the outer leaflet of the plasma membrane during apoptosis. Leveraging the modularity of the BASHY platform, the azido-substituted BASHY dye **9** (Fig. 9) was engineered to tag annexin V *via* strain-promoted azide–alkyne cycloaddition, resulting in the fluorescent bioconjugate **14** (Fig. 15A). This construct was shown to effectively label apoptotic HeLa cells (Fig. 15B).[67]

BASHY-pyridinium for the bioimaging of astrocytes

Cationic fluorophores have been shown to stain astrocytes as they express organic cation transporters that allow the transport of neurotransmitters in the brain.[75] In this study, BASHY dye **8** was engineered to contain a cationic pyridinium moiety on the BA module (Fig. 16) in order to label organotypic cerebellar slice cultures. The slices were incubated with dye **8** and then immunostained for the astrocyte-specific glial fibrillary acidic protein (GFAP). Confocal fluorescence microscopy studies showed that dye **8** co-localized with GFAP in more than 70% of the stained area. This dye displayed 4-fold higher co-localization with astrocytes than the non-cationic dye **15** (Fig. 16).[63]

Therapeutic applications of the BASHY platform

Fluorescent BASHY linker for a GV1001–bortezomib conjugate

The construction of targeted drug conjugates, such as antibody–drug or small molecule–drug conjugates, is often hindered by the complexity of the linker technology, which must ensure both structural stability in circulation and controlled drug release at the target site.[76,77] Additionally, intracellular trafficking studies require bioconjugates to be fluorescent, typically by replacing the cytotoxic drug or incorporating fluorophores into the linker, both of which present drawbacks. An alternative approach is the design of inherently fluorescent linkers.[78,79] Due to the suitable bioimaging properties of BASHY dyes, this platform was re-engineered to develop fluorescent cytotoxic bioconjugates (Fig. 17).[80]

The FDA-approved proteasomal inhibitor bortezomib (Btz) was chosen to be incorporated into the BASHY framework, while retaining the dye's photophysical properties [BASHY **4a** (λ_{abs} = 425 nm, λ_f = 504 nm, Φ_f = 0.10) *versus* BASHY-Btz **16** (λ_{abs} = 412 nm, λ_f = 490 nm, Φ_f = 0.02); in toluene]. Then, BASHY-Btz **16** was coupled with a cell-penetrating peptide, GV1001. The resulting conjugate **17** demonstrated improved cytoplasmic availability as verified by confocal fluorescence microscopy studies. Moreover, it exhibited improved potency against HT-29 cancer cells (IC_{50} = 100 nM) compared to non-vectorized BASHY-Btz **16** (IC_{50} = 450 nM), which showed accumulation in lipid droplets (Fig. 17). The findings of this study revealed that the BASHY platform allows the intracellular tracking of the drug conjugate, promotes the release of the cytotoxic cargo upon hydrolysis and elucidates the chemotherapy resistance mechanism associated with the entrapment of drugs in lipid droplets, which tend to be overexpressed in cancer cells.[80]

BASHY as a PS platform for PDT

In oncology, PDT has emerged as a promising treatment modality that uses light-sensitive compounds, known as PSs, to target and destroy malignant cells. When activated by light of a specific wavelength, these PSs generate reactive oxygen species (ROS) that induce local cell damage.[81,82] Based on the ability of the BASHY dyes **4a–c** (Fig. 6) and **10** (Fig. 9) to generate $^1O_2$ upon light activation (see above), these dyes were tested as PSs for PDT.[64] BASHY **4c** was observed to be the most efficient singlet-oxygen PS [Φ_Δ – **4a** (0.23); **4b** (0.20); **4c** (0.78); in toluene] and exhibited high phototoxicity against the human

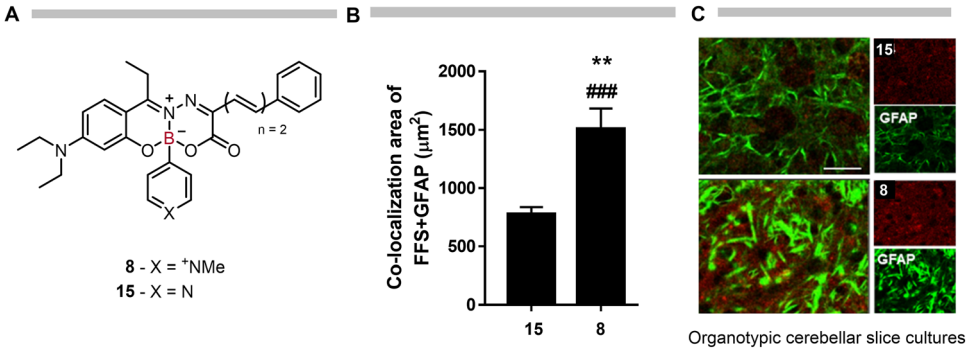

Fig. 16 (A) Structure of the BASHY dyes **8** (cationic) and **15** (neutral); (B) percentage of dye area that co-stains with GFAP; (C) representative images of slices stained with BASHY dyes **8** and **15** (red) and immunostained for GFAP (green). Adapted from ref. 63 with permission from John Wiley and Sons, Copyright 2020.

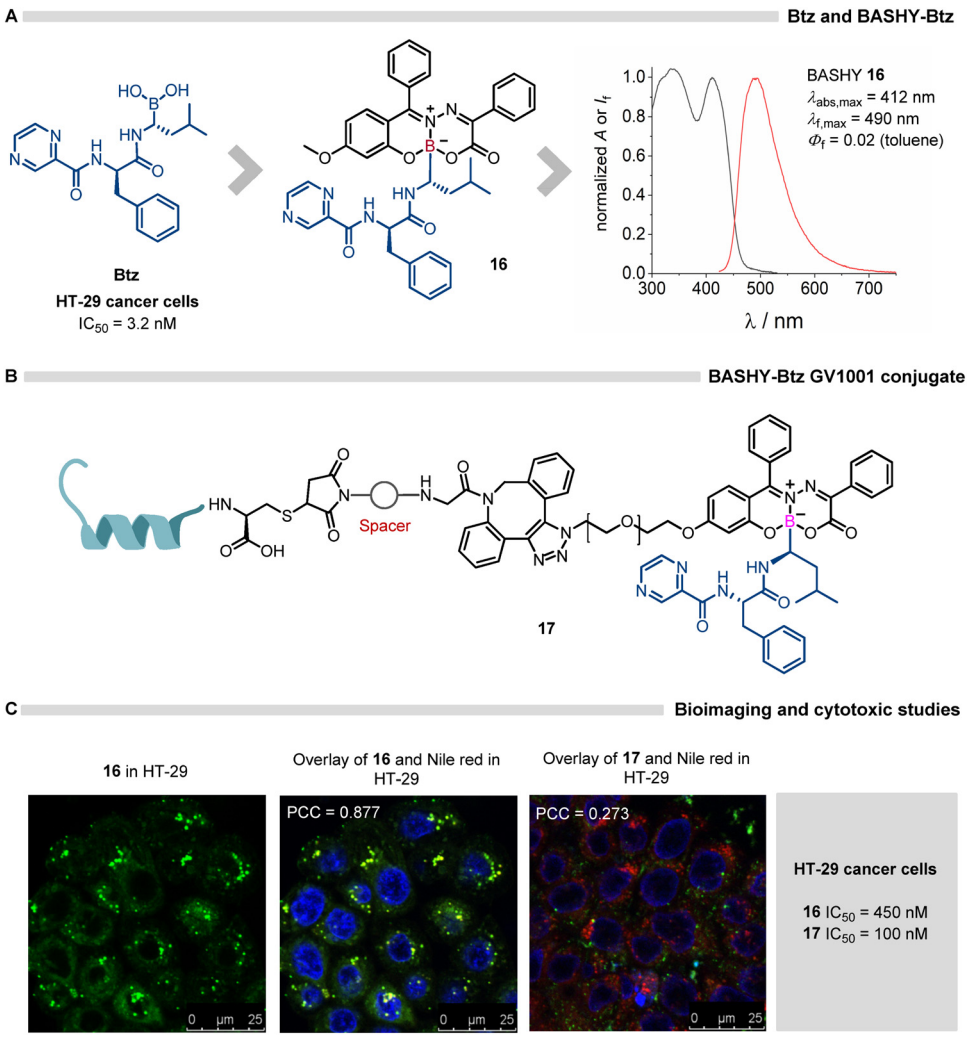

Fig. 17 (A) IC_{50} of Btz in HT-29 cancer cells, along with the structure and optical spectra (UV/vis absorption in black and fluorescence in red) of BASHY-Btz **16**; (B) structure of the fluorescent targeted drug conjugate **17**; (C) cellular staining, co-localization, and cytotoxic evaluation of compounds **16** and **17** in HT-29 cancer cells. Adapted from ref. 80 with permission from American Chemical Society, Copyright 2022.

glioblastoma multiform U87 cell line, with an IC_{50} value in the low nanomolar range (4.40 nM). This was accompanied by an astonishing phototoxicity index (PI $>$ 22 700). BASHY **4c** was shown to accumulate in LDs and this intracellular distribution was found to be essential for the enhanced phototoxicity and induction of ferroptosis by lipid peroxidation (LPO; Fig. 18).[64]

Building on the promising potency and high PI observed in cellular PDT experiments, the safety of dye **4c** was evaluated

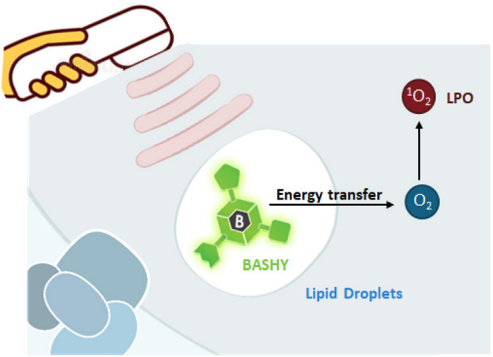

	$^{dark}IC_{50}$ (μM)	$^{light\ 540\ nm}IC_{50}$ (nM)	PI
U87 MG cell line			
4a	>100	14260 ± 780	>7
4b	>100	27.9 ± 1.5	>3600
4c	>100	4.4 ± 0.2	>22700
10	>100	98 ± 17	>1000
PPIX	4.93 ± 1.18	521 ± 94	9.5

Fig. 18 BASHY as a promising PS platform for PDT that targets LDs and triggers ferroptosis. Adapted from ref. 64 with permission from American Chemical Society, Copyright 2023.

in vivo using zebrafish embryos (*Danio rerio*), a well-established toxicity model in preclinical studies.[83,84] BASHY **4c** did not display apparent dark toxicity at concentrations up to 10 μM, in contrast to cisplatin. Subsequent PDT assays demonstrated that at 20 μM, the light irradiation of the PS induced significant morphological abnormalities, such as heart edema, highlighting the potential of the BASHY platform for further *in vivo* phototherapeutic applications.[64]

Current limitations and potential improvements of the BASHY platform

As shown herein, in the course of our research program, we have been able to engineer the BASHY platform in many aspects during the evolution of the various generations of dyes. This includes the improvement of their robustness against hydrolytic stability,[68] the further shift of their emission properties into the red spectral window (600–650 nm),[63] and the addition of stimuli-responsive functionalities.[65]

However, there is still ample room for further evolution of the physicochemical properties related to:

(a) the solubility in water (synthetic modification with potentially water-solubilizing groups, such as sulfonates or carboxylates),

(b) the photostability in general and especially against the oxidation of the polymethine chain in Cy-BASHY by $^1O_2$,

(c) the displacement of the emission properties into the near-infrared spectral region (>700 nm) by further extending the π-framework.

Work on these aspects is currently progressing in our research groups.

Conclusions

The inherent complexity of biological systems and the need to understand the intricate mechanisms that govern their functions have pushed the boundaries of requirements on fluorescent dyes in modern imaging applications. As the demand for higher sensitivity, specificity, and functional adaptability grows, so does the need for innovative chromophore architectures with finely tuned photophysical properties. To address these challenges, MCRs have emerged as powerful tools for the direct and efficient generation of structurally diverse fluorophores, capable of meeting the evolving demands of advanced bioimaging technologies.

The BASHY platform is a structurally and functionally versatile class of BA-derived fluorophores with significant potential for bioimaging and therapeutic applications. Through rational design and modular synthesis, these dyes exploit the coordination of π-conjugated salicylidenehydrazone ligands to a central sp^3-hybridized boron atom, resulting in stable, three-dimensional fluorescent complexes. The most important features of BASHY dyes are their lipophilicity and suitable photostability, combined with large Stokes shifts, polarity-sensitive emission, 2PA properties and high quantum yields in non-polar environments. Furthermore, the modularity of the scaffold enables fine-tuning of photophysical properties through systematic variation of electronic structure and optimization of hydrolytic stability. Importantly, the BA moiety in the BASHY framework allows, in most cases, structural derivatization without altering or compromising the fluorescence output. These features underscore the exceptional modularity and photophysical tunability of the BASHY platform, highlighting its potential for advanced bioimaging applications.

BASHY dyes have demonstrated considerable utility across diverse bioimaging contexts. These include selective accumulation in lipid-rich subcellular compartments such as LDs, which are overexpressed in cancer cells, labeling of astrocytes, which have wide implications in neurochemical processes, fluorescent tagging of apoptotic cells through bioconjugation with annexin V and targeted staining of myelin debris in models of demyelination. Notably, BASHY **4a** enabled *in vivo* imaging of demyelinated brain regions in an EAE mouse model, underpinning the translational potential of this platform in research on neuroinflammation and multiple sclerosis. The BASHY scaffold has also been adapted for advanced microscopic techniques such as FLIM, where medium-dependent lifetime enabled visualization of dynamic vesicle trafficking between cells. In addition to imaging, BASHY dyes show great promise in therapeutic applications. BASHY derivatives demonstrated the ability to sensitize $^1O_2$ formation with high efficiency, particularly BASHY **4c**, which showed strong phototoxicity in

the human glioblastoma multiform U87 cell line (IC_{50} = 4.40 nM) and a suitable *in vivo* safety profile in zebrafish models, validating its application potential in PDT.

Furthermore, the BASHY framework has been successfully integrated into a fluorescent drug conjugate, exemplified by the GV1001–BASHY–bortezomib construct (**17**). This conjugate exhibited potent cytotoxic activity against HT-29 cancer cells (IC_{50} = 100 nM), with the BASHY moiety acting simultaneously as a fluorescent tracking unit and a responsive linker, thereby enabling real-time monitoring of drug delivery.

Overall, the BASHY platform stands out as a modular chromophore technology that covers both diagnostic and therapeutic domains. Its chemical flexibility, robust fluorescence behavior, and demonstrated compatibility with cellular and *in vivo* models position BASHY dyes as promising candidates for next-generation imaging and theranostic agents.

Author contributions

F. M. F. S.: writing – original draft, review & editing. F. G. B.-C.: writing – review & editing. U. P.: funding acquisition, project administration, writing – review & editing. P. M. P. G.: funding acquisition, project administration, writing – review & editing.

Conflicts of interest

The authors declare no conflicts of interest.

Data availability

This feature article did not generate or analyse any new experimental or computational data.

Acknowledgements

The authors are grateful for funding from the Spanish Ministry of Science, Innovation, and Universities (MCIU/AEI/10.13039/501100011033) and the European Regional Development Fund ERDF (grant PID2023-152556NB-I00 to U. P. and pre-doctoral contract PRE2023-001520 to F. G. B.-C.). The authors also acknowledge funding from the Research Institute for Medicines (iMed.ULisboa), which is supported by the Fundação para a Ciência e a Tecnologia (FCT), Portuguese Agency for Scientific Research. iMed.ULisboa is funded by FCT through projects UID/04138/2025 (https://doi.org/10.54499/UID/04138/2025); UID/PRR/04138/2025 (DOI: https://doi.org/10.54499/UID/PRR/04138/2025); and UID/PRR2/04138/2025 (DOI: https://doi.org/10.54499/UID/PRR2/04138/2025). FCT is also thanked for the project grants LISBOA2030-FEDER-00719700 (DOI: https://doi.org/10.54499/2023.16337.ICDT) and 2023.14170.PEX (DOI: https://doi.org/10.54499/2023.14170.PEX). F. M. F. S. also thanks FCT for the CEEC grant (2021.04125.CEECIND).

References

1 Y. Zheng, R. Cai, K. Wang, J. Zhang, Y. Zhuo, H. Dong, Y. Zhang, Y. Wang, F. Deng, E. Ji, Y. Cui, S. Fang, X. Zhang, H. Huang, K. Zhang, J. Wang, G. Li, X. Miao, Z. Wang, Y. Yang, S. Li, J. B. Grimm, K. Johnsson, E. R. Schreiter, L. D. Lavis, Z. Chen, Y. Mu and Y. Li, *Science*, 2025, **388**, eadt7705.
2 L. Wang, M. S. Frei, A. Salim and K. Johnsson, *J. Am. Chem. Soc.*, 2019, **141**, 2770–2781.
3 L. D. Lavis, *Biochemistry*, 2017, **56**, 5165–5170.
4 G. Jiang, H. Liu, H. Liu, G. Ke, T. Ren, B. Xiong, X. Zhang and L. Yuan, *Angew. Chem., Int. Ed.*, 2024, **63**, e202315217.
5 W. Xu, Z. Zeng, J.-H. Jiang, Y. Chang and L. Yuan, *Angew. Chem., Int. Ed.*, 2016, **55**, 13658–13699.
6 A. S. Klymchenko, *Acc. Chem. Res.*, 2023, **56**, 1–12.
7 A. S. Klymchenko, *Acc. Chem. Res.*, 2017, **50**, 366–375.
8 A. Sharma, P. Verwilst, M. Li, D. Ma, N. Singh, J. Yoo, Y. Kim, Y. Yang, J. Zhu, H. Huang, X. Hu, X. He, L. Zeng, T. D. James, X. Peng, J. L. Sessler and J. S. Kim, *Chem. Rev.*, 2024, **124**, 2699–2804.
9 Y. Tanaka, M. Taki and S. Yamaguchi, *Chem. Commun.*, 2025, **61**, 1164–1167.
10 M. Hirai, N. Tanaka, M. Sakai and S. Yamaguchi, *Chem. Rev.*, 2019, **119**, 8291–8331.
11 X. Liu and Y. Chang, *Chem. Soc. Rev.*, 2022, **51**, 1573–1591.
12 S. Munan, Y. Chang and A. Samanta, *Chem. Commun.*, 2024, **60**, 501–521.
13 C. Lim, D. Seah and M. Vendrell, *Chem. Soc. Rev.*, 2026, **55**, 1352–1370.
14 S. Benson, F. de Moliner, W. Tipping and M. Vendrell, *Angew. Chem., Int. Ed.*, 2022, **61**, e202204788.
15 F. de Moliner, N. Kielland, R. Lavilla and M. Vendrell, *Angew. Chem., Int. Ed.*, 2017, **56**, 3758–3769.
16 G. Hong, A. L. Antaris and H. Dai, *Nat. Biomed. Eng.*, 2017, **1**, 0010.
17 K. Grover, A. Koblova, A. T. Pezacki, C. J. Chang and E. J. New, *Chem. Rev.*, 2024, **124**, 5846–5929.
18 J. H. Choi, S. Kim, O. Kang, S. Y. Choi, J. Y. Hyun, H. S. Lee and I. Shin, *Chem. Soc. Rev.*, 2024, **53**, 9446–9489.
19 L. D. Lavis and R. T. Raines, *ACS Chem. Biol.*, 2014, **9**, 855–866.
20 J. V. Jun, D. M. Chenoweth and E. J. Petersson, *Org. Biomol. Chem.*, 2020, **18**, 5747–5763.
21 L. Levi and T. J. J. Müller, *Chem. Soc. Rev.*, 2016, **45**, 2825–2846.
22 L. Brandner and T. J. J. Müller, *Front. Chem.*, 2023, **11**, 1124209.
23 I. Saridakis, M. Riomet, O. J. V. Belleza, G. Coussanes, N. K. Singer, N. Kastner, Y. Xiao, E. Smith, V. Tona, A. de la Torre, E. F. Lopes, P. A. Sánchez-Murcia, L. González, H. H. Sitte and N. Maulide, *Angew. Chem., Int. Ed.*, 2024, **63**, e202318127.
24 A. Loudet and K. Burgess, *Chem. Rev.*, 2007, **107**, 4891–4932.
25 D. Frath, J. Massue, G. Ulrich and R. Ziessel, *Angew. Chem., Int. Ed.*, 2014, **53**, 2290–2310.
26 A. M. Comiskey and E. V. Anslyn, *J. Org. Chem.*, 2025, **90**, 7161–7167.
27 R. R. Groleau, T. D. James and S. D. Bull, *Coord. Chem. Rev.*, 2021, **428**, 213599.
28 H. Reyes, B. M. Muñoz, N. Farfán, R. Santillan, S. Rojas-Lima, P. G. Lacroix and K. Nakatani, *J. Mater. Chem.*, 2002, **12**, 2898–2903.
29 R. Chan-Navarro, V. M. Jiménez-Pérez, B. M. Muñoz-Flores, H. V. R. Dias, I. Moggio, E. Arias, G. Ramos-Ortíz, R. Santillan, C. García, M. E. Ochoa, M. Yousufuddin and N. Waksman, *Dyes Pigm.*, 2013, **99**, 1036–1043.
30 D. G. Hall, *Boronic Acids – Preparation and Applications in Organic Synthesis, Medicine and Materials*, Wiley-VCH Verlag & Co. KGaA, Weinheim, 2011.
31 S. D. Bull, M. G. Davidson, J. M. H. van den Elsen, J. S. Fossey, A. T. A. Jenkins, Y. Jiang, Y. Kubo, F. Marken, K. Sakurai, J. Zhao and T. D. James, *Acc. Chem. Res.*, 2013, **46**, 312–326.
32 D. Wu, A. C. Sedgwick, T. Gunnlaugsson, E. U. Akkaya, J. Yoon and T. D. James, *Chem. Soc. Rev.*, 2017, **46**, 7105–7123.
33 R. Nishiyabu, Y. Kubo, T. D. James and J. S. Fossey, *Chem. Commun.*, 2011, **47**, 1106–1123.
34 Y. Kubo, A. Kobayashi, T. Ishida, Y. Misawa and T. D. James, *Chem. Commun.*, 2005, 2846–2848.
35 H. Reyes, J. M. Rivera, N. Farfán, R. Santillan, P. G. Lacroix, C. Lepetit and K. Nakatani, *J. Organomet. Chem.*, 2005, **690**, 3737–3745.
36 J. F. Lamère, P. G. Lacroix, N. Farfán, J. M. Rivera, R. Santillan and K. Nakatani, *J. Mater. Chem.*, 2006, **16**, 2913–2920.

37 B. M. Muñoz, R. Santillan, M. Rodríguez, J. M. Méndez, M. Romero, N. Farfán, P. G. Lacroix, K. Nakatani, G. Ramos-Ortíz and J. L. Maldonado, *J. Organomet. Chem.*, 2008, **693**, 1321–1334.
38 M. Rodríguez, G. Ramos-Ortíz, M. I. Alcalá-Salas, J. L. Maldonado, K. A. López-Varela, Y. López, O. Domínguez, M. A. Meneses-Nava, O. Barbosa-García, R. Santillan and N. Farfán, *Dyes Pigm.*, 2010, **87**, 76–83.
39 J. Su, F. Chen, V. L. Cryns and P. B. Messersmith, *J. Am. Chem. Soc.*, 2011, **133**, 11850–11853.
40 J. P. M. António, R. Russo, C. Parente Carvalho, P. M. S. D. Cal and P. M. P. Gois, *Chem. Soc. Rev.*, 2019, **48**, 3513–3536.
41 J. P. M. António, I. L. Roque, F. M. F. Santos and P. M. P. Gois, *Acc. Chem. Res.*, 2025, **58**, 673–687.
42 F. M. F. Santos, J. N. Rosa, N. R. Candeias, C. Parente Carvalho, A. I. Matos, A. E. Ventura, H. F. Florindo, L. C. Silva, U. Pischel and P. M. P. Gois, *Chem. – Eur. J.*, 2016, **22**, 1631–1637.
43 W. Dou, H. Han, A. C. Sedgwick, G. Zhu, Y. Zang, X. Yang, J. Yoon, T. D. James, J. Li and X. He, *Sci. Bull.*, 2022, **67**, 853–878.
44 X. Wang, Q. Ding, R. R. Groleau, L. Wu, Y. Mao, F. Che, O. Kotova, E. M. Scanlan, S. E. Lewis, P. Li, B. Tang, T. D. James and T. Gunnlaugsson, *Chem. Rev.*, 2024, **124**, 7106–7164.
45 N. Chen, W. Zhang, S. Chen, Q. Wu, C. Yu, Y. Wei, Y. Xu, E. Hao and L. Jiao, *Org. Lett.*, 2017, **19**, 2026–2029.
46 J. Wang, X. Fang, X. Guo, Q. Wu, Q. Gong, C. Yu, E. Hao and L. Jiao, *Org. Lett.*, 2021, **23**, 4796–4801.
47 M. Ibarra-Rodríguez, B. M. Muñoz-Flores and V. M. Jiménez-Pérez, *J. Lumin.*, 2018, **198**, 342–349.
48 M. Ibarra-Rodríguez, B. M. Muñoz-Flores, R. Chan-Navarro, N. Waksman, A. Saucedo-Yañez, M. Sánchez and V. M. Jiménez-Pérez, *Opt. Mater.*, 2019, **89**, 123–131.
49 M. López-Espejel, M. Ibarra-Rodríguez, B. M. Muñoz-Flores, M. R. Bahena-Villarreal, A. A. Cavazos-Jaramillo, M. D. Garza-Villegas, C. Rodríguez-Padilla, I. E. Luna-Cruz, H. V. R. Dias, J. M. Alcocer-González and V. M. Jiménez-Pérez, *New J. Chem.*, 2023, **47**, 7975–7985.
50 C. Yu, G. Di, Q. Li, X. Guo, L. Wang, Q. Gong, Y. Wei, Q. Zhao, L. Jiao and E. Hao, *Inorg. Chem.*, 2024, **63**, 21397–21409.
51 L. Wang, Y. Sun, C. Yu, W. Ma, Y. Shang, L. Ding, T. Wang, X. Guo, J. Zhang, Y. Li, E. Hao, G. Wang and L. Jiao, *Org. Lett.*, 2025, **27**, 8551–8556.
52 M. Ibarra-Rodríguez, B. M. Muñoz-Flores, H. V. R. Dias, M. Sánchez, A. Gomez-Treviño, R. Santillan, N. Farfán and V. M. Jiménez-Pérez, *J. Org. Chem.*, 2017, **82**, 2375–2385.
53 M. Ibarra-Rodríguez, B. M. Muñoz-Flores, A. Gómez-Treviño, R. Chan-Navarro, J. C. Berrones-Reyes, A. Chávez-Reyes, H. V. R. Dias, M. Sánchez Vázquez and V. M. Jiménez-Pérez, *Appl. Organomet. Chem.*, 2019, **33**, e4718.
54 J. Jia and J. Wen, *Tetrahedron Lett.*, 2021, **71**, 153006.
55 E. B. Kömüşdoğan, S. Batool, E. Şahin, E. Yildirim, M. Işık and C. Tanyeli, *Chem. Commun.*, 2025, **61**, 576–579.
56 B. Tharmalingam, R. Kishore Kumar, O. Anitha, W. Kaminsky, J. G. Malecki and B. Murugesapandian, *Dalton Trans.*, 2025, **54**, 3897–3910.
57 S. Guieu, C. I. C. Esteves, J. Rocha and A. M. S. Silva, *Molecules*, 2020, **25**, 6039.
58 H. Wang, X. Guo, W. Bu, Z. Kang, C. Yu, Q. Wu, L. Jiao and E. Hao, *Dyes Pigm.*, 2023, **210**, 111013.
59 V. Savickienė, A. Bieliauskas, S. Belyakov, E. Arbačiauskienė and A. Šačkus, *Molecules*, 2024, **29**, 3432.
60 D. H. McDaniel and H. C. Brown, *J. Org. Chem.*, 1958, **23**, 420–427.
61 M. M. Alcaide, F. M. F. Santos, V. F. Pais, J. I. Carvalho, D. Collado, E. Pérez-Inestrosa, J. F. Arteaga, F. Boscá, P. M. P. Gois and U. Pischel, *J. Org. Chem.*, 2017, **82**, 7151–7158.
62 A. D. Laurent, B. Le Guennic and D. Jacquemin, *Theor. Chem. Acc.*, 2016, **135**, 173.
63 F. M. F. Santos, Z. Domínguez, J. P. L. Fernandes, C. Parente Carvalho, D. Collado, E. Pérez-Inestrosa, M. V. Pinto, A. Fernandes, J. F. Arteaga, U. Pischel and P. M. P. Gois, *Chem. – Eur. J.*, 2020, **26**, 14064–14069.
64 M. J. S. A. Silva, Y. Zhang, R. Vinck, F. M. F. Santos, J. P. M. António, L. Gourdon-Grünewaldt, C. Zaouter, A. Castonguay, S. A. Patten, K. Cariou, F. Boscá, F. Nájera, J. F. Arteaga, G. Gasser, U. Pischel and P. M. P. Gois, *Bioconjugate Chem.*, 2023, **34**, 2337–2344.
65 J. Felicidade, F. M. F. Santos, J. F. Arteaga, P. Remón, R. Campos-González, H. Nguyen, F. Nájera, F. Boscá, D. Y. W. Ng, P. M. P. Gois and U. Pischel, *Chem. – Eur. J.*, 2023, **29**, e202300579.
66 F. M. F. Santos, Z. Domínguez, M. M. Alcaide, A. I. Matos, H. F. Florindo, N. R. Candeias, P. M. P. Gois and U. Pischel, *ChemPhotoChem*, 2018, **2**, 1038–1045.
67 P. M. S. D. Cal, F. Sieglitz, F. M. F. Santos, C. Parente Carvalho, A. Guerreiro, J. B. Bertoldo, U. Pischel, P. M. P. Gois and G. J. L. Bernardes, *Chem. Commun.*, 2017, **53**, 368–371.
68 J. M. J. M. Ravasco, J. Felicidade, M. V. Pinto, F. M. F. Santos, R. Campos-González, J. F. Arteaga, M. Mehraz, C. Langevin, A. Fernandes, H. Nguyen, D. Y. W. Ng, J. A. S. Coelho, U. Pischel and P. M. P. Gois, *JACS Au*, 2024, **4**, 4212–4222.
69 M. Pawlicki, H. A. Collins, R. G. Denning and H. L. Anderson, *Angew. Chem., Int. Ed.*, 2009, **48**, 3244–3266.
70 V. G. Jiménez, F. M. F. Santos, S. Castro-Fernández, J. M. Cuerva, P. M. P. Gois, U. Pischel and A. G. Campaña, *J. Org. Chem.*, 2018, **83**, 14057–14062.
71 A. Zadoorian, X. Du and H. Yang, *Nat. Rev. Endocrinol.*, 2023, **19**, 443–459.
72 K. M. Monroe and G. Di Paolo, *Nat. Neurosci.*, 2021, **24**, 451–452.
73 M. V. Pinto, F. M. F. Santos, C. Barros, A. R. Ribeiro, U. Pischel, P. M. P. Gois and A. Fernandes, *Cells*, 2021, **10**, 3163.
74 B. Torrado, B. Pannunzio, L. Malacrida and M. A. Digman, *Nat. Rev. Methods Primers*, 2024, **4**, 80.
75 A. N. Preston, J. D. Farr, B. K. O'Neill, K. K. Thompson, S. E. Tsirka and S. T. Laughlin, *ACS Chem. Biol.*, 2018, **13**, 1493–1498.
76 V. Kostova, P. Désos, J. Starck and A. Kotschy, *Pharmaceuticals*, 2021, **14**, 442.
77 J. D. Bargh, A. Isidro-Llobet, J. S. Parker and D. R. Spring, *Chem. Soc. Rev.*, 2019, **48**, 4361–4374.
78 B. Lee, C. Chalouni, S. Doll, S. C. Nalle, M. Darwish, S. P. Tsai, K. R. Kozak, G. Del-Rosario, S. Yu, H. Erickson and R. Vandlen, *Bioconjugate Chem.*, 2018, **29**, 2468–2477.
79 D. Xiao, L. Zhao, F. Xie, S. Fan, L. Liu, W. Li, R. Cao, S. Li, W. Zhong and X. Zhou, *Theranostics*, 2021, **11**, 2550–2563.
80 S. Baldo, P. Antunes, J. F. Felicidade, F. M. F. Santos, J. F. Arteaga, F. Fernandes, U. Pischel, S. N. Pinto and P. M. P. Gois, *ACS Med. Chem. Lett.*, 2022, **13**, 128–133.
81 D. E. J. G. J. Dolmans, D. Fukumura and R. K. Jain, *Nat. Rev. Cancer*, 2003, **3**, 380–387.
82 T. Mishchenko, I. Balalaeva, A. Gorokhova, M. Vedunova and D. V. Krysko, *Cell Death Dis.*, 2022, **13**, 455.
83 F. M. Richards, W. K. Alderton, G. M. Kimber, Z. Liu, I. Strang, W. S. Redfern, J. Valentin, M. J. Winter and T. H. Hutchinson, *J. Pharmacol. Toxicol. Methods*, 2008, **58**, 50–58.
84 N. Mandrekar and N. L. Thakur, *Biotechnol. Lett.*, 2009, **31**, 171–179.

